Electron plasmas: Confinement and mode structure in a small aspect ratio toroidal experiment

S. Pahari, H. S. Ramachandran, and P. I. John

Citation: Physics of Plasmas (1994-present) **13**, 092111 (2006); doi: 10.1063/1.2345584
View online: http://dx.doi.org/10.1063/1.2345584
View Table of Contents: http://scitation.aip.org/content/aip/journal/pop/13/9?ver=pdfcov
Published by the AIP Publishing

Electron plasmas: Confinement and mode structure in a small aspect ratio toroidal experiment

S. Pahari[a)]
Institute for Plasma Research, Bhat, Gandhinagar, 382428, India

H. S. Ramachandran[b)]
Indian Institute of Technology, 600 036, Madras, India

P. I. John
Institute for Plasma Research, Bhat, Gandhinagar, 382428, India

(Received 16 February 2006; accepted 24 May 2006; published online 15 September 2006)

Toroidal electron plasmas have remained less explored due to their poor confinement properties. Their equilibrium, stability, and confinement properties are therefore not entirely understood and continue to remain a topic of intense ongoing research. Large aspect-ratio theory suggests poor confinement in toroidal devices can be overcome by the application of a radial electric field; this has been verified successfully in some of the recent experiments. In the present paper, we report the longest confinement time without these external forces. Increasing the toroidicity has helped us to generate these forces intrinsically. To this end, a trap to confine electron plasmas has been created in a small aspect-ratio (≈ 1.6) torus. Electrons after being injected from a thermionic source are seen to remain confined with a purely toroidal magnetic field. The confinement time is far more than known single particle drift time scales. Importantly, it is in the absence of any external electric field, additional rotational transform, and/or magnetic fields, which, although not required, in principle, may appear essential particularly due to their role in improving confinement in some of the recent large aspect-ratio traps. The successful confinement in the small aspect-ratio limit has also led to several interesting observations: the evolution of the confined plasma is marked by an interesting nonlinear (large amplitude), electrostatic wave activity. Coherent, periodic, double peak oscillations result from a low-frequency $\mathbf{E}\times\mathbf{B}$ motion of a toroidal vortex in a plasma that closely leans against the inner wall. As many as 16 highly phase-coherent harmonics with dominant power in $m=2$ suggest that the mode is not merely a center-of-charge motion. Rather, a strong coupling of modes leads to a novel nonlinear state. The predominant energy is present in the shaping of the electron cloud ($m=2$) and not in the displacement of the center of charge ($m=1$) seen in large aspect-ratio traps. The absence of any power-law tail suggests absence of any turbulence, at least on time scales longer than the wall-probe resolution (40 ns). The frequency, (around 100 kHz at 200 G) shows an unusual shear in time: it reduces as the mode evolves, but later increases as the mode dies. © *2006 American Institute of Physics*. [DOI: 10.1063/1.2345584]

I. INTRODUCTION

Magnetized electron plasmas, in cylindrical geometries,[1,2] have excellent confinement properties. Therefore their equilibrium, stability, and mode structures have been extensively investigated. In equilibrium, the electron cloud has a time-independent profile, and undergoes a self-rotation with all the electrons experiencing $\mathbf{E}\times\mathbf{B}$ drift, where $\mathbf{E}$ is the self-electric (space-charge) field. These plasmas have revealed the existence of both linear and nonlinear modes that are stable or unstable. Most notable among them and of ubiquitous presence are diocotron modes.[3–9] The diocotron mode in its simplest form is a center-of-charge motion. A displacement of the electron cloud from equilibrium causes an extra induced charge on the wall, resulting in a radial electric field, $\mathbf{E_d}$. The resulting $\mathbf{E_d}\times\mathbf{B}$ drift of the center of charge about the axis is in the same direction of the equilibrium drift, though slower. This linear (small amplitude) diocotron mode is a flute mode ($k_z=0$) and has an azimuthal mode number, $m=1$. Nonlinear versions as well as higher mode numbers have also been identified in cylindrical traps and either occur naturally or are externally launched.

Compared to their cylindrical counterparts, toroidal electron plasmas and their mode structure have so far remained less explored due to their poor confinement properties. The toroidal single-particle drifts, namely ∇B and curvature drifts, appear to constrain their confinement, just as they do in the case of toroidal neutral plasmas. The latter, it may be recalled, requires a complex combination of toroidal, poloidal and vertical magnetic (B) fields for their confinement. Equilibrium theory[10] of toroidal electron plasmas, however, predicts that poloidal fields are not essential, since, in the presence of a toroidal B field, the $\mathbf{E}\times\mathbf{B}$ motion arising from the space-charge $\mathbf{E}$ field acts as an effective rotational transform. But a few earlier experiments, on these principles, had resulted in the maximum confinement of barely hundreds of

[a)]Electronic mail: sambaran@ipr.res.in
[b)]Electronic mail: hsr@tenet.res.in

μs.[11–16] Later, theoretical predictions for large aspect-ratio toroids led to the requirement of additional external forces to counteract the forces of self-repulsion and diamagnetism present in these plasmas.[17] A radial external electric field was therefore proposed, analogous to the vertical magnetic field required for the magnetohydrodynamics equilibrium of neutral plasmas. Renewed interest in these plasmas has led to several experiments in recent times,[18–20] where a radial electric field ($\mathbf{E}_{ext}$) has been considered essential and externally imposed. The application of an external electric field by Stoneking *et al.*,[18] has led to confinement up to 2 ms. Additional feedback damping of the poloidal $\mathbf{E}\times\mathbf{B}$ drift has led to further improvement up to 18 ms.[19]In a different set of experiments, Saitoh *et al.*[20] have shown confinement up to 100 ms. Here, in addition to an external electric field a dipole magnetic field has been applied. In the absence of E_{ext}, while Stoneking *et al.* reports no confinement, Saitoh *et al.* reports a short confinement time of about 10 μs. The key, it appears therefore, is the external electric field that has led to successful confinement in these traps in conformity with the theoretical predictions. Improved confinement has also led to observations of low frequency oscillations in these traps. These have been related to the $m=1$ diocotron modes observed in cylindrical geometries and have been used for total charge (Q) measurements, with the frequency of the oscillations given by $f=Q(8\pi^3 Ra^2 B)$, (R being the major radius, a the minor radius, and B the magnetic field at R). Given the large aspect ratio of these traps it is not surprising that the characteristics reported so far (e.g., the mode number, the nonlinear shift in frequency, etc.[19]) appear largely similar to those present in cylindrical (*infinite* aspect-ratio) devices.[5]

While confinement in large aspect-ratio toroidal traps have gained ground, the mode structure and evolution of electron plasmas in the limit of small aspect-ratio, although equally interesting, continue to remain a less explored regime of significant fundamental interest. With increase in toroidicity the difference between the inner and outer wall area increases, leading to stronger induced electric fields on the walls. This can have interesting consequences for confinement and evolution. Spatial inhomogeneity in $\mathbf{B}$ breaks down the incompressible nature of fluid and in tight aspect-ratio toroids, these effects can get more pronounced due to strong gradients in $\mathbf{B}$. A coupling of modes can also be expected. Overall, the theoretical approximations that relate the large aspect-ratio toroidal geometries to cylindrical geometries are no more expected to be valid in the limit of a small aspect ratio.

The results presented in this paper are from a SMall Aspect Ratio Toroidal EXperiment in a C-shaped trap (SMARTEX-C) with $\varepsilon=R_0/a\sim 1.6$ (ε=aspect ratio, R_0=major radius, a=minor radius). Electrons after being injected thermionically along the field lines are confined between two negatively biased grids placed poloidally at two toroidal locations, 300° apart; the broken toroidal symmetry gives the trap a C shape as in Refs. 18 and 19. Radial confinement is via a (pulsed) toroidal magnetic field. SMARTEX-C employs an injection-hold-dump mechanism along the field lines, *a la* cylindrical traps. Wall probes, mounted flush with the walls, are capacitively coupled to the plasma and are used to measure image currents. The information carried by these induced currents is interpreted through an appropriate model to provide information on the plasma activity. A charge collector provides additional useful information about the total charge content and its time evolution. Experiments in SMARTEX-C indicate that toroidal electron plasmas, in the limit of strong toroidicity, have intrinsic confinement properties and a unique mode structure. Successful confinement, for several hundred diocotron oscillations without any external electric field, has been demonstrated for the first time. Confinement in SMARTEX-C has also led to investigations of toroidal electrostatic flute modes that result from a low-frequency $\mathbf{E}\times\mathbf{B}$ motion of a coherent object. Several interesting features are seen that set the mode apart from conventional diocotron modes. The mode is not merely a center-of-charge motion. Rather, a strong coupling of modes leads to a novel, nonlinear state with an interesting mode structure. Among other things, it turns out that $m=2$ is the dominant mode in SMARTEX-C, as opposed to $m=1$ seen in conventional, large aspect-atio machines. Also, the time evolution is marked by a nonmonotonic shear in frequency, hitherto unseen in linear or large aspect-ratio machines.

The SMARTEX-C setup and diagnostics have been described in Sec. II. The mode and its features have been presented in Sec. III. The confinement properties have been discussed in Sec. IV. Vortex dynamics has been modeled to obtain the time evolution of a vortex charge; this is discussed and compared with the total charge evolution in the plasma in Sec. V. The spectral analysis of the mode, including the power spectrum and frequency evolution is presented in Sec. VI. We conclude the paper with a discussion on the experimental findings in Sec. VII.

II. EXPERIMENTAL SETUP

The experiments in SMARTEX-C have been carried out at the Institute for Plasma Research (IPR), Gandhinagar, India, and are a continuation of earlier small aspect-ratio experiments at IPR, referred in Refs. 13–16. The earlier set of experiments were performed in a similar but toroidally continuous device (SMARTEX-T); fuelling of the plasma was achieved through cross-field injection. In SMARTEX-C the toroidal symmetry has been broken to allow injection along the magnetic field lines. Langmuir Probes of SMARTEX-T have been replaced with newer and improved diagnostics. The vacuum, instrumentation and data acquisition have also been suitably upgraded. SMARTEX-C is therefore an improved and modified version of SMARTEX-T.

A. Design of trap

The SMARTEX-C device is shown in Fig. 1. The plasma chamber is a torus with a rectangular cross section. The inner radius of the vacuum chamber is 2.5 cm. A second inner wall is placed at a radius of 5 cm and acts as the inner wall for the plasma. The outer wall is at 22 cm. This yields an aspect ratio ($=R_0/a$) of 1.6, with R_0 (major radius) =13.5 cm and a (minor radius) =8.5 cm. The chamber is 32 cm in height. It

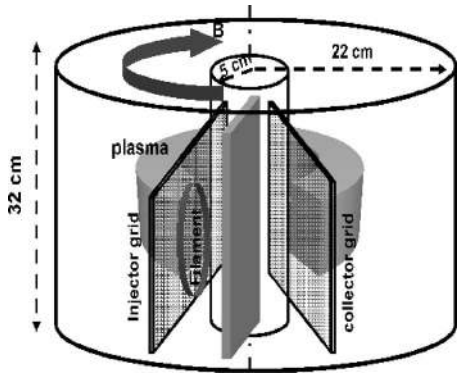

FIG. 1. SMARTEX-C Trap: a three-dimensional (3-D) diagram showing the locations of the Filament, the Injector Grid, and Collector Grid.

is maintained in ultrahigh vacuum conditions $\leq 10^{-7}$ Torr. A single circular tungsten filament loop of diameter 10 cm is placed on a poloidal cross section. The filament emits electrons thermionically when a current of approximately 18 A is passed through it. It is biased to 330 V negative with respect to ground. A grid (injector) placed in front of the filament is biased initially to −400 V, 70 V more negative than the filament. Another grid (collector) placed behind the filament in the poloidal cross section, is also biased to −400 *V*. The toroidal symmetry is thus broken. The trapping parameters are shown in Fig. 2. A toroidal magnetic field is established in the chamber by pulsing a current through a 28 turn coil. The pulsed magnetic field has an overall duration of about 4.5 ms and a flat top of roughly 1 ms. As the *B* field reaches its flat top, the injector grid is pulsed to 0 V (+330 V with respect to filament) for 60 μs. Electrons are thereby injected along the field lines. Thereafter the grid reverts back to −400 V, ensuring no further fueling. The injected electrons are now trapped toroidally between the negatively biased injector grid and collector grid. Radial confinement is achieved through the toroidal magnetic field.

The rise time of the injector grid is about 30 ns and the fall time is within 100 ns. These times are well below the $\mathbf{E}\times\mathbf{B}$ times, but the fall time is comparable to the Trivelpiece-Gould transit time[21] for the device. The relatively slow fall time is not important since the filament remains on, and the situation is analogous to the appearance of a barrier between two regions of a magnetic bottle that are already in equilibrium with each other.

All biases, pulse widths, and delays that define the magnetic field, injector-grid bias and collector-grid bias traces can be suitably varied and synchronized electronically by means of a trigger circuit. The trap therefore is similar to a Penning-Malmberg trap[1,2] or toroidal C-trap[18] but retains strong toroidal features.

B. Diagnostics

Capacitive probes and a charge-collector have so far been the mainstay of SMARTEX-C.

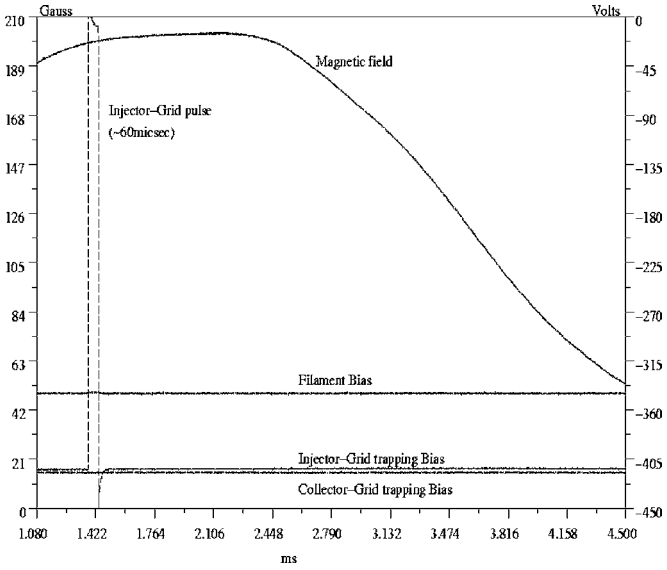

FIG. 2. Injection and Trapping parameters: The Injection pulse: ~345 V with respect to the Filament, applied on the Injector Grid for 60 μs, after a delay of ~1.5 ms after the *B* field is triggered.

1. Capacitive probes

Capacitive probes[22] are disk probes, 4.6 cm in diameter, mounted flush with the walls of the device. These probes appear as part of the wall, but are insulated from the rest of the wall. A single wall probe is placed at midplane on the inner wall at 120° toroidally. Five wall probes are placed, 5.4 cm apart, on the inner wall at 240°. A probe has also been placed on the outer wall at 240°. All probes are identical in design and grounded through a 1 KΩ resistor. As they are capacitively coupled to the plasma, induced charges flow to and fro and the resulting currents are measured. These currents can be interpreted to obtain information about the evolution of the plasma. An appropriate model, consistent with the complex plasma dynamics, has been developed to interpret the wall-probe currents and estimate the charge content in the vortex. The wall probes therefore serve as a useful non-invasive diagnostic.

2. Charge collector

Total charge measurements in the plasma have been carried out using the collector grid. The grid can be pulsed to ground at any instant (with a rise time of 50 ns) to dump the electrons (dump studies). The resulting current from the collector to the ground is measured with a Current Transformer and integrated to obtain the charge held in the trap at the instant of dump. Such charge measurements pose several challenges due to complexities of the trap. A small aspect ratio and inward shifted equilibrium cause fast transit times to the collector. Charges are of the order of nano-Coulombs, as such plasmas are tenuous. The presence of strong pickups due to capacitive coupling of the collector and the grounded vessel further complicates the measurements. Thus a charge collector with high sensitivity, fast response time, and appropriate shielding was designed to reliably obtain the time-resolved information of the total charge content in the plasma (Q total).

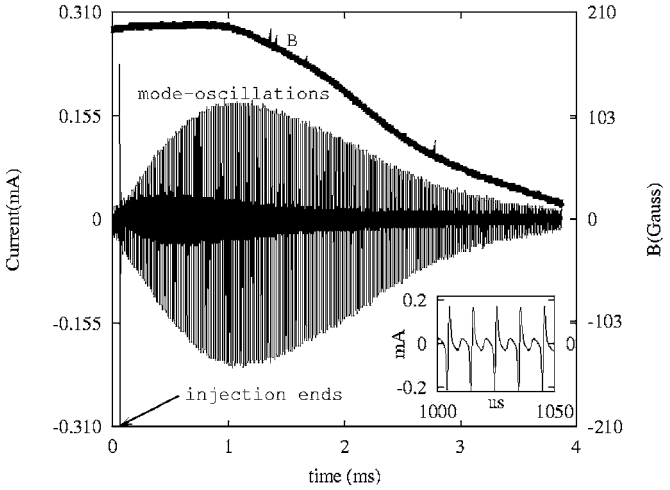

FIG. 3. Voltage oscillations as seen across a 1 K resistor on a capacitive probe, mounted on the midplane at 120° from the source. Also shown is the B field ~200 G. The Inset shows a close-up of the oscillations.

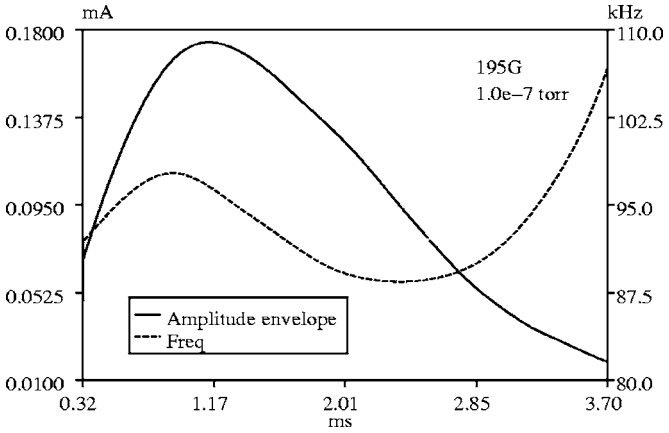

FIG. 4. The amplitude envelope of the mode is obtained from the peak-instantaneous currents of the oscillations. The inverse of the time instances of these peaks gives the frequency of the mode.

Further details of the trap and the design of the charge collector are being deferred for another appropriate journal.

III. MODE AND ITS FEATURES

Earlier experiments have shown that the natural equilibrium of the plasma in a tight aspect-ratio device takes the form of a D-shaped plasma hugging the inner wall.[13,14] Our injector (filament) is, however, mounted along the minor axis. Injection takes place along the field lines and the initial plasma is localized to the cross-sectional presence of the circular injecting filament and corresponds to a hollow cylinder. As the voltage on the injector grid is brought back to −410 V, injection stops. The plasma is now toroidally trapped between the injector grid and the collector grid and evolves via cross-field flows. As the perpendicular rearrangement convects the cylinder, wall probes on the inner and outer walls of the trap pick up long lasting electrostatic oscillations.

A. Basic features

Figure 3 shows a typical plasma shot. The curve at the top of the figure shows the time evolution of the magnetic field. The other curve is the signal picked up by one of the inner-wall probes placed on the midplane at 240° from the injector grid. The early noisy portion of 60 μs corresponds to the injection period. Once injection is turned off, extremely coherent, periodic oscillations appear that gradually grow in amplitude and then decay, lasting right into the decay phase of the magnetic field. This wall probe signature is seen over a wide range of pressures and magnetic fields.

A closer look [Fig. 3 (inset)] shows that the oscillations are extremely coherent, periodic and have two alternating cycles with different peak amplitudes in a single period. The period, roughly seen to be ~10 μs, slowly drifts in time. The peaks in every oscillation represent the peak instantaneous currents induced on the wall probe. These peaks, traced together, give the time evolution of the amplitude of the mode. Also, the inverse of the time instances of occurrence of these peaks gives a rough estimate of the frequency. The time evolution of the amplitude and frequency so obtained are shown for a typical evolution in Fig. 4.

The wall probes are capacitively coupled to the plasma; the oscillations on the probes therefore represent electrostatic wave activity. To prove that the oscillations are not an artifact or noise, a 50 ns pulse on the collector grid, after about 250 μs of confinement, is used to dump the plasma. This causes the electrons to flow out along the field lines onto the grounded collector. The mode is seen to get killed (Fig. 5) with this pulse, clearly affirming that the oscillations are indeed due to plasma activity.

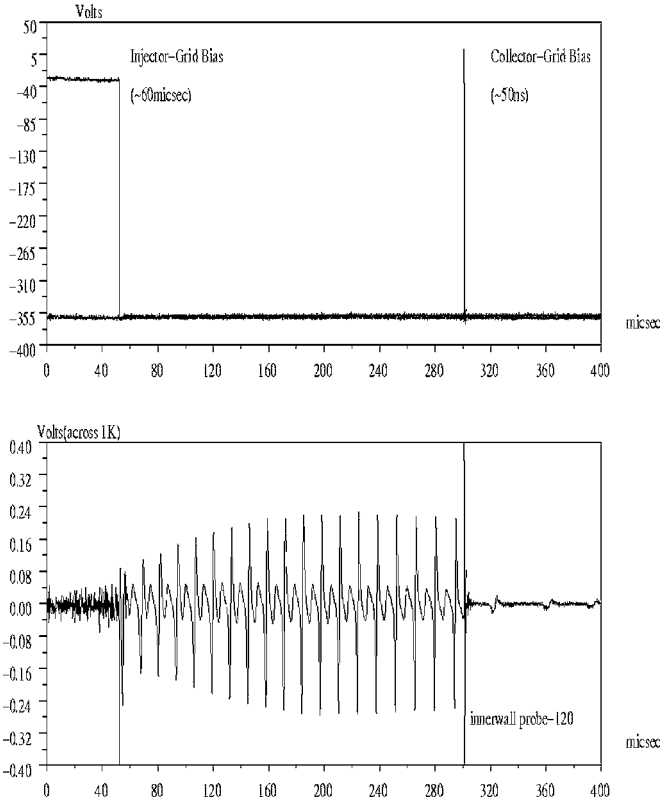

FIG. 5. Dumping the plasma onto collector grid kills the mode.

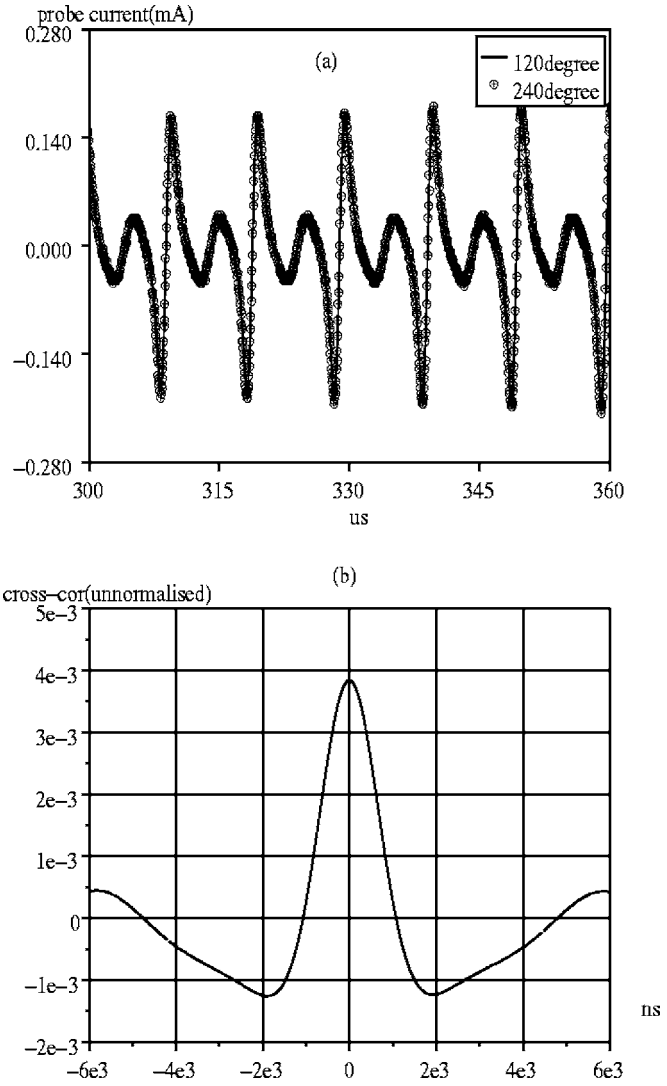

FIG. 6. (a) Oscillations on Toroidally placed probes (on the midplane) on the inner wall at 120° and 240°; (b) cross-correlation of the same.

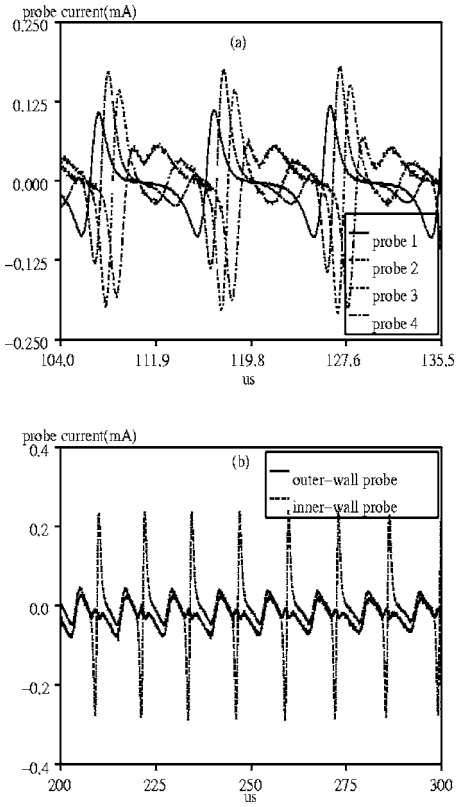

FIG. 7. (a) Mode seen by poloidal probes on the inner wall at 240°; probe1, probe2: above the midplane, probe3: on the midplane, probe4: below the midplane. (b) The mode seen by probes placed on the inner and outer wall (at the midplane) (the outer-wall probe signal is scaled by 10, for clarity).

B. $k_\perp$ mode

The mode structure of these oscillations is investigated, through the simultaneous acquisition of signals from wall probes placed at different toroidal and poloidal locations, on the inner and outer walls of the trap. Two toroidally separated probes (120° and 240°) register equally large signals that are synchronous [Fig. 6(a)]. Cross-correlation of these wall probe signals also confirms that $k_\parallel=0$ [Fig. 6(b)]. On the other hand, Fig. 7(a) shows a time delay between oscillations on four adjacent poloidal probes placed inboard, 5.4 cm apart. Correlating the traces from the poloidal probes shows that the vortex is traveling from top to bottom near the inner wall, consistent with the B field direction. Simultaneous measurements made with probes on the inner and outer wall (on the midplane) show a phase difference of 180° [Fig. 7(b)]. All these suggest that the wave activity that dominates the post-injection period is strongly flute-like in nature. The sharp oscillations indicate a coherent structure sweeping past the wall probe. That is, the zeroth order **E** resulting from the image charges on the inner wall crossed with (a nonuniform) **B** results in the low-frequency poloidal motion, which is picked up by the wall probes as periodic oscillations.

C. "Double-peak" oscillations

The $k_\perp$ nature of the observations do confirm that the mode is $\mathbf{E}\times\mathbf{B}$ drift phenomena of a toroidal vortex, like the well-known diocotron mode observations in linear machines. However, the oscillations are marked by several other interesting signatures.

Compared to inboard probes, an outer wall probe signal is weaker by a factor ≈ 50 [Fig. 7(b)]. This implies an inward shift in the position of the cloud. This is consistent with earlier observations of a D-shaped plasma closely hugging the inner wall in small aspect-ratio machines. Interestingly, a single oscillation, representing one complete poloidal rotation, is seen to consist of two alternating cycles (see Fig. 3-inset). We believe that the double peak in the oscillations results from an elliptical trajectory of the vortex.

The inward shift of the cloud together with a rectangular cross section of the device would allow the trajectory to become elliptical or D-shaped (in the poloidal plane). To present this idea in greater detail, a qualitative schematic is shown in Fig. 8. A single oscillation seen by a capacitive probe on the midplane is shown [Fig. 8(a)]; alongside the plasma is represented by contours with a toroidal vortex [Fig. 8(b)]. In an elliptic trajectory close to the inner wall, it

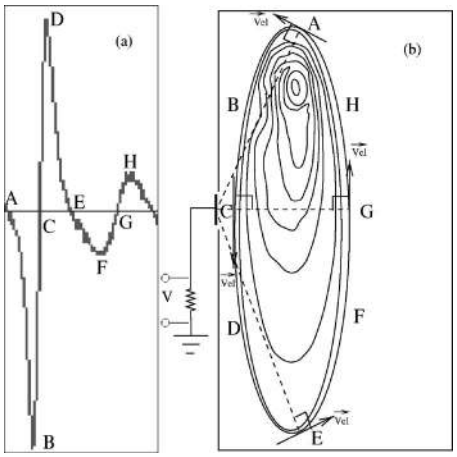

FIG. 8. A schematic showing a single period of oscillation resulting from one azimuthal drift, (a) a single period of oscillation, (b) the plasma profile depicted in the poloidal cross section.

is evident from the schematic that the coherent object induces similar currents in the wall probe twice—once during its passage along the inner wall past the probe and again during its return passage when it drifts through the same z locations. The transit past the wall probe (on its way down) is represented by the large oscillating current signal represented as A–E in Fig. 8(a). As the vortex comes closer to the probe (A–C) the induced charges flow into the wall-probe from ground, producing a negative current. As it moves away (C–E), a positive current is produced. This repeats itself, on the return path E–A, resulting in the second, weaker oscillating signal. The amplitude is weaker since the structure, during the return path, is farther away and hence the strength of the induced current is smaller due to less capacitive coupling and less induced electric field normal to the probe. In effect, there are four points in the D-shaped orbit where the distances from the probe to the point go through extrema, giving rise to two maxima (and two minima) and therefore two alternating cycles. These are points when the velocity vector will be perpendicular to the line joining the probe to the point. In contrast, for a circular motion, as seen in linear machines, the signal is roughly inversely proportional to the distance from the probe to the density peak and this distance has a single minimum and a single maximum, i.e., a single alternating cycle. The latter has been reported from weakly toroidal systems[19] too.

The traces from the probes that are 5.4 cm above and below the midplane are roughly mirror reflections about the midplane. However, the part of the signal that marks the return path of the vortex (E–A in Fig. 8) is seen to be quite different on different poloidal probes [Fig. 7(a)]. This is expected as a convective vortical object in a toroidal (inhomogeneous) B field, is squeezed as it $\mathbf{E}\times\mathbf{B}$ drifts to near the inner wall, and spreads out as it drifts away. Its spatial extent and shape is therefore a function of its radial position, which, in turn, is a function of the orbital(z) position during the return path (for a D-shaped plasma).

D. Velocity of vortex

A cross-correlation analysis of poloidal probe signals brings to the forefront another feature: a fast movement near the inner wall is followed by a slower movement away from it. When traces from adjacent poloidal probes are correlated with each other [Figs. 9(a)–9(d)], it is found that delays of between 700 and 900 ns are required to bring the steep portion of the traces into coincidence. This corresponds to a velocity of 6×10^4 to 8×10^4 m/s. However, delays of 1400 to 1800 ns are required to bring the smaller peaks into coincidence, corresponding to speeds of 3×10^4 to 4×10^4 m/s. The structure therefore is seen to move far more slowly on its return trip, E–A, than along its passage along the inner wall.

Since the distance between neighboring probes is known (5.4 cm), the velocity near the inner wall at any instant can also be estimated from the time taken by the vortex to travel between two probes. The latter is known from the time interval between the corresponding peaks on neighboring probes. The time evolution of velocity so obtained is plotted in Fig. 10 for different B. Interestingly, the vortex motion always saturates with a maximum poloidal drift velocity of 70 km/s near the inner wall, irrespective of B. The transit velocities are also found to be almost constant between all adjacent inner-wall probes. [This is the justification for drawing the region A–E in Fig. 8(b) as a straight line.] An alternate means of computing the velocity of the vortex is to measure the time between peaks "B" and "D." At "B," the bottom of the structure is level with the top of the probe and at "D" its top is level with the bottom of the probe. This calculation yields the same velocity mentioned above. What this also means is that the size of the coherent object is smaller compared to the probe's diameter, which is 4.6 cm.

IV. CONFINEMENT OF PLASMA

The presence of large amplitude electrostatic modes permits us to put a lower bound on plasma lifetime. At pressures $\approx8\times10^{-8}$ Torr the plasma appears to last for around 400 diocotron oscillations and the lifetime is seen to extend well past 3 ms (Fig. 3). Collisional effects at higher pressures degrade the confinement. It has been further observed that the interior of the plasma chamber must have no symmetry-breaking elements, such as mechanical design imperfections or even Langmuir probes. They greatly degrade the plasma lifetime and affect the modes.

The confinement time increases further with lower pressures and/or higher magnetic fields. However, with the present magnetic field limited to a flat top of ~1 ms, it is not possible presently to quote an accurate lifetime of the plasma, as it rather seems to get affected by the limited duration of the pulsed magnetic field. But when compared to the maximum possible time scales due to single-particle toroidal drifts (~400 μs for $B=200$ G and minimum assumed $T_e=1$ eV), the observed confinement time is much longer. This confirms that the plasma is indeed contained by strong collective effects.

Importantly, this confinement is in the absence of any external electric field. From the velocity computed in Sec.

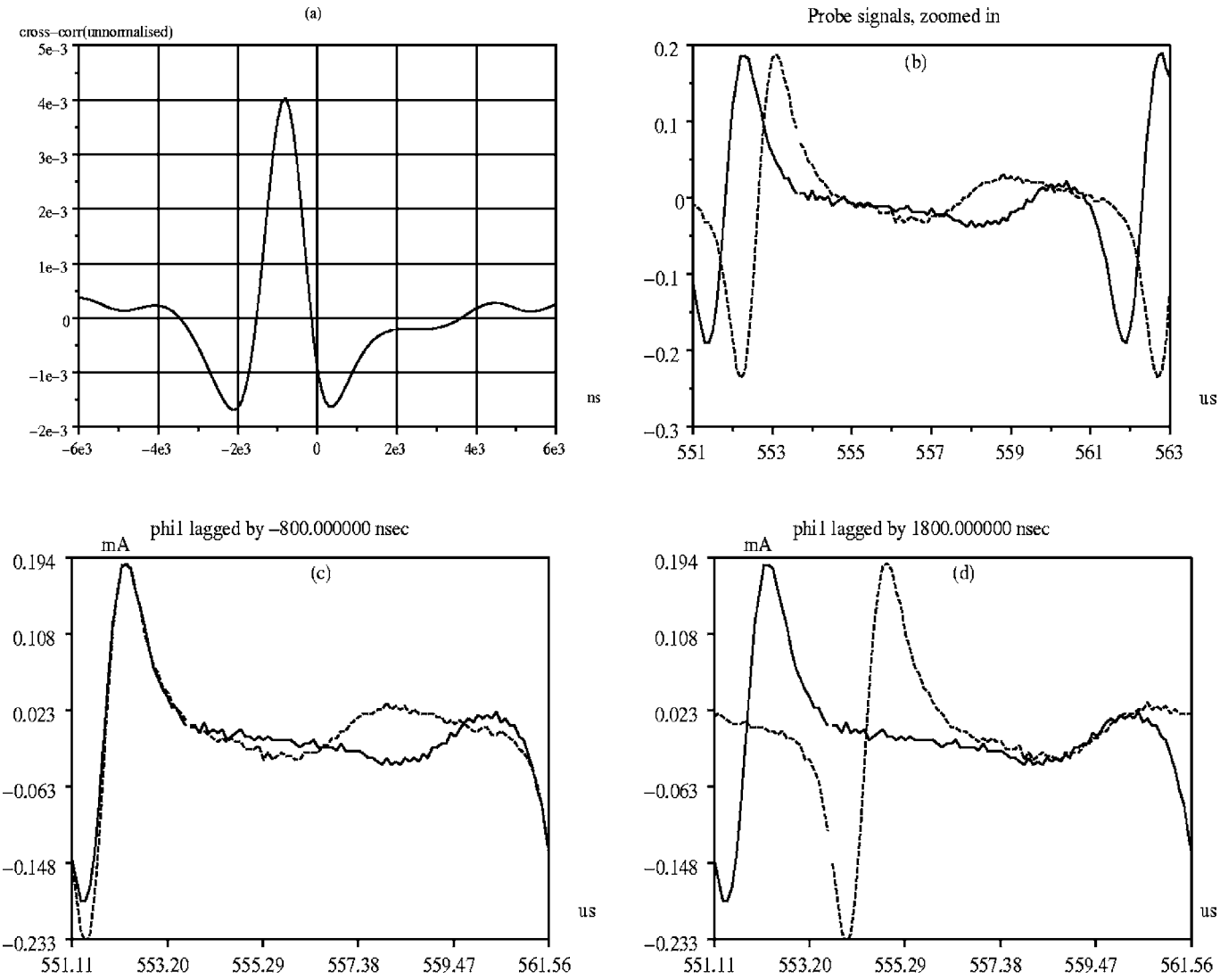

FIG. 9. (a) Cross-correlation of two signals from poloidal probes; (b) probe signals shown over approximately one oscillation period; (c) big peaks (movement near inner wall) synchronize when shifted by 800 ns; (d) small peaks (movement near outer wall) synchronize when shifted by 1800 ns.

III D and B (on the inner wall) known ($\approx$440 G), an electric field of 3 kV/m is estimated on the inner wall. This field is generated self-consistently due to the image charges. So, in the limit of a small aspect ratio, the intrinsic electric fields can be substantially strong, enough to support the plasma without any E_{ext}.

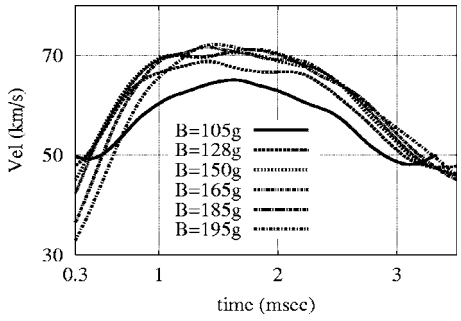

FIG. 10. Time evolution of the vortex velocity (near inner wall) computed from the poloidal probe signals.

The long-lasting confinement is independently confirmed from the dump studies that gives the time evolution of the total charge, Q_{total}, in the plasma. This has been discussed next.

V. CHARGE ESTIMATION

The evolution of Q_{total}, as obtained from dumps onto the charge collector, has been shown in Fig. 11 (bold line). The total charge rapidly decays in the first 10 μs (Fig. 11-inset). During this period half the charge is thrown out and Q_{total} drops from $\approx$8 to 4 nC. Thereafter, it decays slowly, with the plasma lasting well past 3 ms. For comparison, the time evolution of vortex charge (Q_{vortex}), as estimated from the wall probes (for similar conditions), have also been shown in Fig. 11 (dotted lines).

Here Q_{vortex} is obtained from the wall probe data by means of the following analysis. The wall probe data has indicated a flute like structure. We therefore view the object as a charge ring. However, as it is toroidally confined by barrier potentials, the toroidal ring is not a full ring. The flute

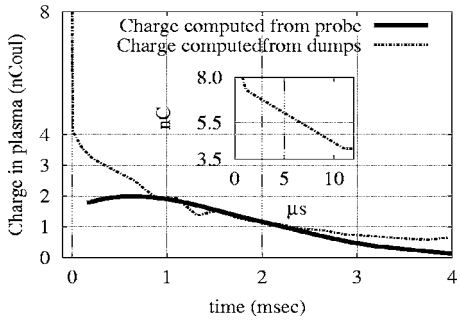

FIG. 11. Time evolution of vortex charge through the wall probe measurements (Q_{vortex}) and total charge through dump studies (Q_{total}). Both curves correspond to a magnetic field of 200 G. Inset: the time evolution of Q_{total} in the first 10 μs.

nature of the signals, however, permits us to assume θ independence. Second, poloidally spaced wall probes pick up signals that are delayed by a constant amount, which is interpreted to mean that the structure moves with constant velocity near the inner wall. Third, the extremely sharp rise in the wall probe signal, coupled with delay, indicates that the plasma extent is at most the size of the probes themselves. For example, Fig. 7(a) shows that the currents in the next and previous probes are substantially down at the time that it peaks in a particular wall probe. This could only be the case if the plasma extent was smaller than inter probe distances ($\sim$5 cm). All the above allow us to view the object as a vortex ring that is θ independent and executing D-shaped excursions in $r-z$.

Since the vortex is so close to the inner wall, almost all the induced wall charge is on the inner wall, and it too is a ring that moves in step with the vortex. As the vortex sweeps past a wall probe, the induced charge wave also sweeps past the same probe. In fact, the charge on the wall probe at any instant is nothing but the integration over the probe area of this induced charge wave. Thus, we may write

$$Q_p(t) = \int_{\theta_1}^{\theta_2} \int_{z_1(\theta)}^{z_2(\theta)} \sigma_W(z,t) a \, dz \, d\theta, \tag{1}$$

where the integral is over the probe surface, σ_W is the surface charge density of the induced charge wave, and Q_P is the total induced charge on the wall probe. Since almost all of the induced charge is on the inner wall, at each time t,

$$2\pi a \int_{z_{\min}}^{z_{\max}} \sigma_W(z,t) dz \approx Q, \tag{2}$$

where Q is the charge induced on the inner wall, a is the radius of the inner wall, and z_{min} and $z_{\max}$ are well below and well above the probes. As the vortex sweeps past the probe, it also changes shape. However, the very sharp peaks imply that whatever the shape changes, the vortex remains sharply localized and translates with uniform velocity in z. Thus, the image charges are well modeled, as fixed in shape; additionally they have been observed to move with constant velocity, v_0 (Sec. III D). This makes σ_W translation invariant, i.e.,

$$2\pi a \int_{z_{\min}}^{z_{\max}} \sigma_W(z - v_0 t, 0) dz = 2\pi a v_0 \int_{t_1}^{t_2} \sigma_W(z_0 - v_0 t, 0) dt \approx Q. \tag{3}$$

Thus, integrating over the time that the charge ring sweeps down from the top to the bottom of the inner wall, we get [using Eqs. (1) and (3)],

$$\int_{t_1}^{t_2} Q_P \, dt = \int_{\theta_1}^{\theta_2} \int_{z_1(\theta)}^{z_2(\theta)} \int_{t_1}^{t_2} \sigma_W(z,t) dt \, a \, dz \, d\theta = \frac{Q}{2\pi a v_0} \int_{\theta_1}^{\theta_2} \int_{z_1(\theta)}^{z_2(\theta)} a \, dz \, d\theta = \frac{Q}{2\pi a v_0} A_P, \tag{4}$$

where A_p is the area of the wall probe.

Now to estimate Q from Eq. (4) the current oscillations on the wall probe are integrated to give the charge induced on it, Q_p. To further integrate Q_p, one needs to know t_1 and t_2. The portion *ABCDE* in Fig. 8(a) roughly represents the transit down the inner wall. We have therefore assigned $t_1 = t_A$ and $t_2 = t_E$. Velocity, v_0, near the inner wall is obtained from poloidal probes on the inner wall (Sec. III D). Since area of probes (A_p) and the wall radius (a) are known, one can compute the total charge, Q, induced on the inner wall. This, in turn, is equivalent to charge content in the vortex, Q_{vortex}.

A small correction, however, needs to be introduced due to the broken toroidal symmetry. The total length of the plasma column (along θ) induces a charge ring on the inner wall which is less than $2\pi a$ due to the presence of injector and collector assembly. This assembly occupies around 1/6 of the toroidal assembly. The retarding potentials on the trapping grids further reduce the plasma length by an estimated 10%–15%. The computed charge is therefore *less* by an equivalent factor, estimated to be $\approx$30%. That is, Q estimated from Eq. (4) is corrected by a factor of 0.7 to give actual charge induced on the inner wall, which as we understand, mostly reflects Q_{vortex}. Another weakness of the result is the fact that as the vortex sweeps past the inner wall, it also changes shape. However, given that the midplane probe is at the symmetry plane, the vortex is nearly stationary in shape when it sweeps past that probe. It is also true that the vortex is slowly changing in charge content, and this aspect is not taken into account in the above derivation. Finally, velocity is strictly constant only near the inner wall. So while integrating in time from A to E, we have included small regions of the trajectory (on the edges) that are not quite constant in velocity, since A and E are more toward the outboard. The region of constant velocity is therefore an approximation. At present we do not have a way of identifying this region more accurately. Since these regions, near the edges, are small, we expect their contribution to be small, and accordingly the error in charge computation will not be so significant. In spite of these approximations, this model yields a simple and robust expression that links the charge measured by the midplane wall probe and the vortex charge content.

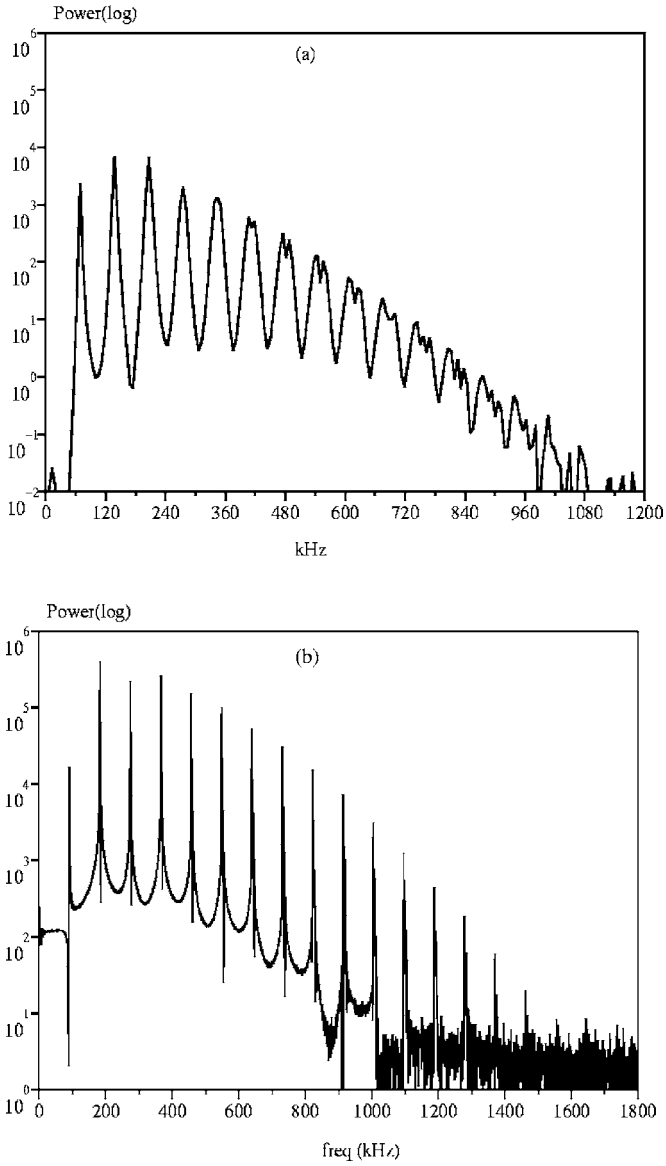

FIG. 12. (a) The amplitude spectrum of the wall-probe signal over a small window of data (40 μs:56 μs) corresponding roughly to 16 diocotron periods. (b) The amplitude spectrum of the complete wall-probe signal after "time warping."

VI. SPECTRAL ANALYSIS

From inspection, the vortex oscillations are seen to be locally periodic whose characteristics slowly vary in time. Because of this time shear in frequency, peaks are smeared out and standard FFT (of the complete signal) to obtain the power spectrum proves inadequate. One can therefore try local Fourier transforms using a window function. Twelve harmonics are visible [see Fig. 12(a)], but the higher harmonics are smeared out due to the shear in the fundamental frequency of the mode. Additionally, windowing assumes that the signal is periodically extended, which does not properly represent the real signal. Further, reducing the size of the window reduces the resolution of the spectrum. Clearly, windowed Fourier analysis does not deal well with periodic signals whose characteristics are varying in time.

A better approach is to include our knowledge of the signal by using model based estimation. We choose a small enough window of data such that the frequency does not vary much. In the current analysis, we fitted a Fourier series in an unknown fundamental frequency, with harmonics up to a maximum cutoff frequency. The cutoff frequency, ω_c, was chosen to be about 20 times the fundamental:

$$f(t;\omega,A_1,\ldots,B_N) = A_0 + \sum_{n=1}^{N} A_n \cos(n\omega t) + \sum_{n=1}^{N} B_n \sin(n\omega t). \tag{5}$$

To ensure that the estimation problem was well conditioned, the data was low pass filtered to the cutoff frequency, and then subsampled at the Nyquist rate corresponding to that cutoff, before estimation was carried out. The fitting is done as a nonlinear minimization problem in a single parameter, namely the unknown frequency ω. For a given ω, the problem of finding the optimal set of $\{A_i\}_{i=1}^{N}$ and $\{B_i\}_{i=1}^{N}$ is a simple problem of linear Least Squares minimization. The residual error is still a function of ω, and is minimized by using a one-dimensional minimizing routine. Each solution is used to guess ω for the next window. Since the time period varied, the window size was adjusted to the local time period. The model order was also adjusted such that the highest harmonic satisfied $N\omega \approx \omega_c$. When this procedure was followed on adaptive windows that were between two and three time periods in extent, a robust estimation algorithm resulted that provided an accurate fit and estimated mode frequency ω accurately over the entire range of acquired data.

It is not necessary that the window represents an integral number of time periods. In practice, only about two to three time periods worth of samples are needed for a good estimate of the parameters. It would seem to be a better approach to fit to a sheared model such as

$$f(t;\omega,\omega',A_1,\ldots,B_N) = A_0 + \sum_{n=1}^{N} A_n \cos(n\omega t + n\omega' t^2) + B_n \sin(n\omega t + n\omega' t^2). \tag{6}$$

However, it is well known that estimating both ω and ω' yields poor results. Estimating the frequency using Eq. (5), and later fitting a smooth curve through the obtained frequencies, yields better results.

A. Power spectrum

One of the primary ways to characterize a stochastic signal is to look at its power spectrum. A standard way to do this is to take the autocorrelation of the signal and take its Fourier transform. However, in a frequency sheared system such as the one present here, this yields little useful information. To get useful information, the local frequency information obtained in the previous section is used to generate a phase function $\phi(t)$. The original signal is sampled uniformly in $\phi(t)$ to yield a set of samples that had no shear.

The resulting power spectrum is shown in Fig. 12(b); the spectral frequencies are now meaningless, but as many as 16

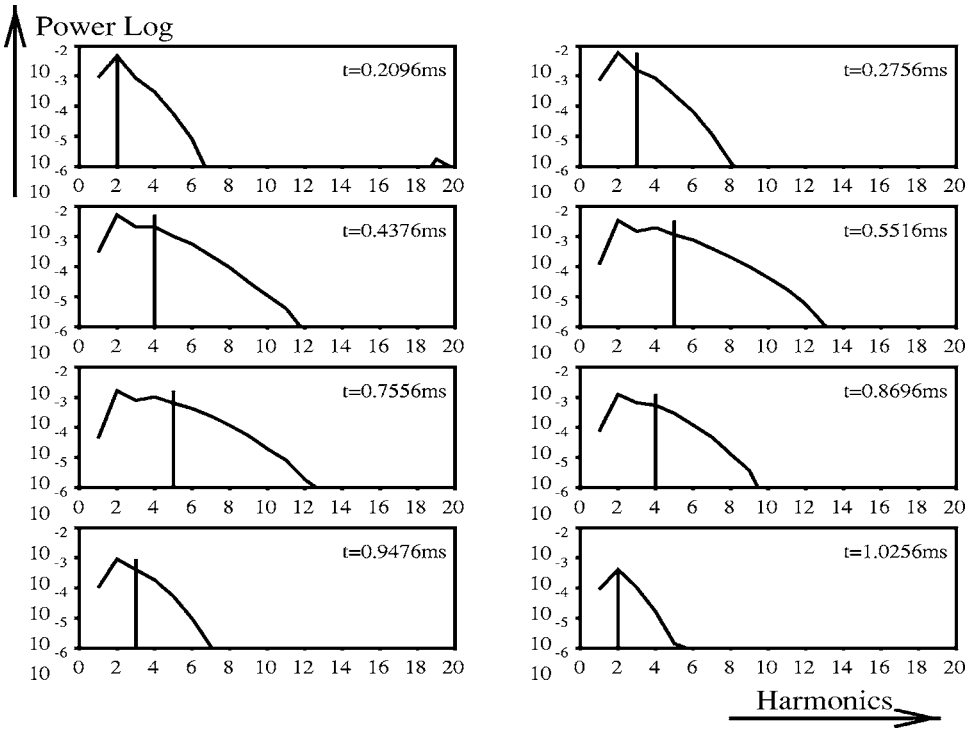

FIG. 13. Snapshots of time evolution of the power spectrum.

harmonics can be clearly seen. As a result of "time warping," the noise floor that was only about 6 dB below the signal, is now nearly 30 dB below. This also confirms that no other low frequency modes of significance are present. Had such modes been present, they would have been smeared out by the above process. However, the resampling process preserves power in these modes, and they would have shown up as noise. The fact that noise is well suppressed by this process confirms the absence of any other low frequency processes. No power-law tail is found in the spectrum, ruling out any turbulence, at least on time-scales observable by the probe (40 ns).

The spectrum shows that the $m=2$ harmonic has the maximum power. Thus, in SMARTEX-C, one sees a coupling of modes with predominant power in the poloidal shaping of the electron cloud that closely hugs the inner wall. This is in sharp contrast to contemporary large aspect-ratio toroidal machines,[19] where $m=1$ mode, resulting from the displacement of the center of charge, is predominant. Our Fourier analysis also confirms that the harmonics are extremely phase coherent.

An interesting observation is how the power distribution between the harmonics evolves in time. Figure 13 shows snapshots of the amplitude spectrum of the mode at different times during a shot. Initially the power is mostly concentrated in the lower harmonics. As the mode evolves, higher harmonics pick up power. Overall power of course decays as the mode decays. In one poloidal drift we do expect that most of the energy is spent in establishing the sharp transition, when the vortex sweeps past the wall probe. The corresponding transit time shown as *B–D* in Fig. 8 should therefore be a dominant feature of this mode. The harmonic whose half period corresponds to this transit time of the vortex (past the wall probe) is indicated in Fig. 13 by a vertical line. The spectra are observed to be flat up to that harmonic and subsequently fall in amplitude. The reason is that lower harmonics see the transit as an impulse, while the higher harmonics see the transit a slowly varying feature.

B. Frequency evolution

The fundamental frequency obtained from the Fourier fit matches exactly with that obtained from the inverse of the peak instants of the oscillations. This is shown for a typical mode evolution in Fig. 14.

The time evolution of fundamental frequency for various operating conditions are shown in Figs. 15(a) and 15(b). The fundamental frequency, on average, increases with a decrease in B [Fig. 15(a)]. On the other hand, it is seen to

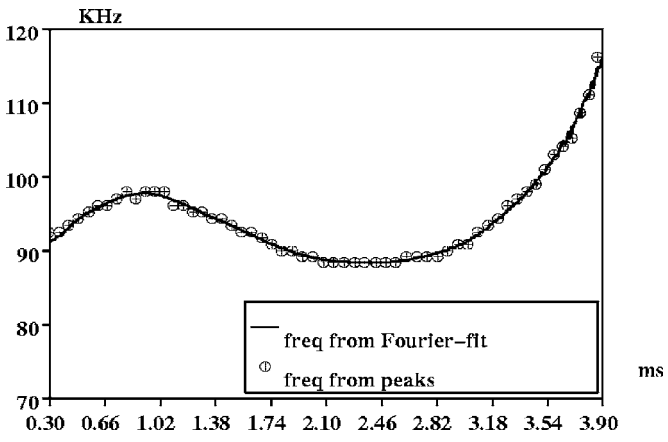

FIG. 14. Frequency obtained from the peaks is overlaid over the fundamental frequency obtained from the Fourier analysis, showing an exact match.

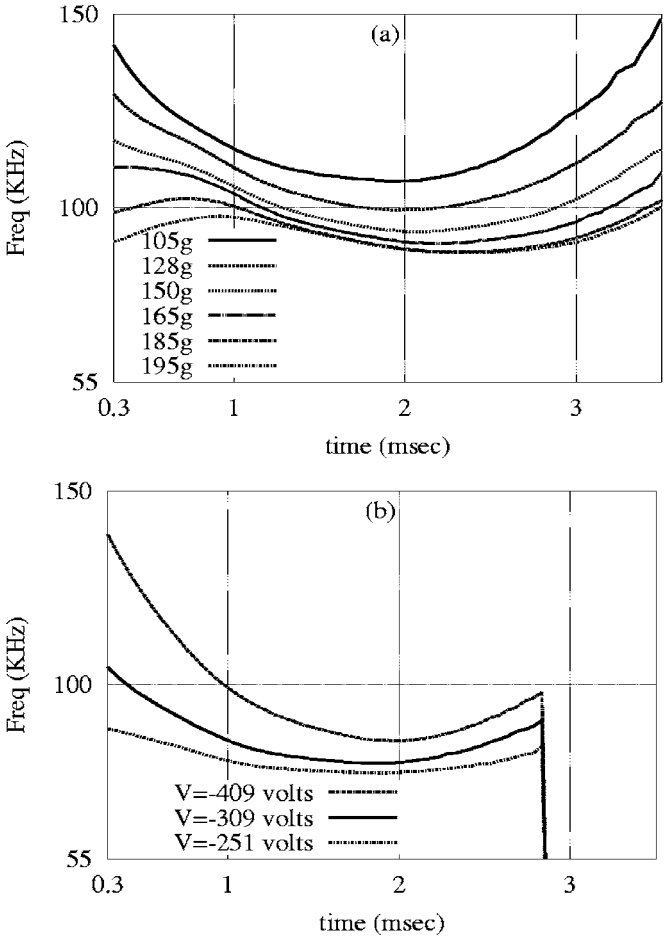

FIG. 15. Frequency evolution (a) for various B, at $V=400$ V (trap potential) and Pressure $=1\times10^{-7}$ Torr; (b) for various V, at $B=150$ G and Pressure $=2.5\times10^{-7}$ T [the early end of the mode in (b) is due to higher pressures that affect the lifetime of the plasma].

increase with the trap potential [Fig. 15(b)]. [In Fig. 15(b) the frequency evolution is marked by an early end as the pressures are high.]

The time evolution of the frequency is peculiar as it shows a strong nonmonotonic shear that is quite different from what has been observed in other linear or toroidal machines. The frequency falls as the mode evolves and again increases as the mode decays. This is true for all B fields. However, with higher B an initial increase in frequency in the initial 1 ms appears. As seen from Fig. 15(a), the shift appears and gradually becomes more pronounced as the field is increased beyond 150 G.

VII. DISCUSSION AND CONCLUSIONS

Experiments in SMARTEX-C have led to observation of several novel features of toroidal electron plasmas. In the limit of small aspect ratio these plasmas are seen to have intrinsic confinement properties and unique mode structure.

The experiments demonstrate that $E\times B$ rotational transform due to self-electric fields and a purely toroidal magnetic field can lead to significant confinement (of more than 3 ms) in toroidal geometries. The confinement time, to the best of our knowledge, is the longest reported so far in the absence of any external (radial) electric field. In the limit of small aspect ratio, due to strong toroidicity, self-consistent electric field induced on the inner wall is sufficiently strong to make any external force field redundant. The confinement time is seen to increase if B increases or pressures in the trap are lowered. A steady state magnetic field will soon be incorporated to increase the confinement time and to scale the plasma lifetime accurately.

It may be noted that theoretical predictions[17] as well as recent experiments[18–20] requiring the presence of E_{ext} are all in the limit of a large aspect ratio. Ref. 17 does suggest that force balance can also be achieved by image charges on a conducting boundary; such a force-balance analysis is presented in detail in Ref. 23. From a theoretical standpoint therefore, the confinement without any $\mathbf{E}_{\text{ext}}$ in SMARTEX-C should not come as a surprise. SMARTEX-C has succeeded in *experimentally demonstrating*, for the first time, the longest confinement in a small aspect-ratio torus, without $\mathbf{E}_{\text{ext}}$. This is important, since SMARTEX-T had reported poor confinement while recent experiments achieved improvement only with external field and explicitly showed that without it plasma decays rapidly. This could have led to an impression that external force field is quintessential.

One must also note that the force-balance analysis, presented in Ref. 23, assumes toroidal symmetry; this does not accurately represent SMARTEX-C which obviously lacks such a toroidal symmetry. What might bother even more is the fact that experiments in SMARTEX-T,[13,14] had failed to achieve similar confinement even though the traps had aspect-ratios same as or lower than SMARTEX-C. The poorer confinement in these experiments, was possibly due to one or more of the following reasons. The pressures were high($>4\times10^{-7}$ Torr); our experiments in SMARTEX-C at these pressures have indicated a rapid decay of the plasma. Furthermore, as discussed in Sec. IV, asymmetries, say, any design imperfections and/or mechanical protrusions (e.g. Langmuir probes) in the interior of the plasma chamber, drastically reduce the lifetime. In SMARTEX-T, Langmuir probes were the principle diagnostics and might have contributed to the poorer confinement; in comparison, SMARTEX-C relies on nonintrusive diagnostics. Besides, SMARTEX-C departs from its predecessor in having injection along the field lines (as in a Penning-Malmberg Trap) and lack toroidal symmetry. It might be, however, early to say if these also contribute to efficient injection and improved confinement, and these issues are currently under investigation.

The nonlinear, electrostatic, $k_\perp$ mode seen in SMARTEX-C is significantly novel. The mode appears extremely early after the injection. When injection ceases, the cylindrical electron cloud, centered about the minor axis, becomes untenable. The unmatched injection initiates a nonlinear (large amplitude), center-of-charge motion ($m=1$), pushing the plasma very close to the inner wall. We believe that this perpendicular rearrangement causes half the charge to be thrown out in one diocotron period. As the plasma rearranges itself closer to the inner wall, the D-shaped plasma results in an elliptic trajectory for the coherent structure; of course, the rectangular cross-section of the trap allows room for this

ellipticity. The elliptic trajectory gives rise to interesting double-peak oscillations on the wall probes. $m=1$ is, however, not the dominant mode. Strong coupling of many modes results in a highly noninear state. The maximum power is in $m=2$; this is a consequence of the shaping of the cloud that is pushed against the inner wall. The absence of any power-law tail suggests the absence of any turbulence on time scales longer than 40 ns, which is the wall probe resolution. A peculiarity of the evolution, seen universally across all pressures and B fields, is the unusual nonmonotonic frequency evolution. In the conventional diocotron mode, nonlinear evolution involves an increase in frequency. This has been seen for both cylindrical and toroidal (large aspect-ratio) geometries.[5,19] The mode observed in SMARTEX-C increases in amplitude (nonlinear growth) while experiencing a drop in frequency. This is especially true for low B fields, although with higher B, frequency slightly increases with an increase in nonlinearity. However, at later times for all B fields, when the mode decays and reduces in nonlinearity, the frequency once again increases.

SMARTEX-C has brought to the forefront several novel properties and, with it, the urgent need to further address these issues with new experiments and theory. The compressibility of fluid in the presence of strong inhomogeneous B brings in an entirely new perspective; all of this may bring in a paradigm shift in the investigations of toroidal electron plasmas. In particular, the amplitude saturation and frequency evolution warrants further understanding of the evolution of the vortex. In a subsequent paper the characterization of the evolution through parametric studies will be presented in detail.

ACKNOWLEDGMENTS

The authors acknowledge the useful discussions held with R. Ramalingam of IIT, Madras with regard to the signal processing of the data. We also thank R. Ganesh, P. K. Chattopadhyay, and P. K. Kaw for many useful comments on the work.

[1] J. H. Malmberg and J. S. deGrassie, Phys. Rev. Lett. **35**, 577 (1975).
[2] J. H. Malmberg and C. S. Driscoll, Phys. Rev. Lett. **44**, 654 (1980).
[3] R. H. Levy, Phys. Fluids **8**, 1288 (1965).
[4] W. D. White, J. H. Malmberg, and C. F. Driscoll, Phys. Rev. Lett. **49**, 1822 (1982).
[5] S. A. Prasad and J. H. Malmberg, Phys. Fluids **29**, 2196 (1986).
[6] K. S. Fine, C. F. Driscoll, and J. H. Malmberg, Phys. Rev. Lett. **63**, 2232 (1989).
[7] C. F. Driscoll, Phys. Rev. Lett. **64**, 645 (1990).
[8] C. F. Driscoll and K. S. Fine, Phys. Fluids B **2**, 1359 (1990).
[9] K. S. Fine and C. F. Driscoll, Phys. Plasmas **5**, 601 (1998).
[10] J. D. Daugherty and R. H. Levy, Phys. Fluids **10**, 155 (1967).
[11] J. D. Daugherty, J. E. Eninger, and G. S. Janes, Phys. Fluids **12**, 2677 (1969).
[12] W. Clark, P. Korn, A. Mondelli, and N. Rostoker, Phys. Rev. Lett. **37**, 592 (1976).
[13] S. S. Khirwadkar, P. I. John, K. Avinash *et al.*, Phys. Rev. Lett. **71**, 4334 (1993).
[14] P. Zaveri, P. I. John, K. Avinash *et al.*, Phys. Rev. Lett. **68**, 3295 (1992).
[15] S. S. Khirwadkar, Ph.D. thesis, Institute for Plasma Research, India, 2002.
[16] P. Zaveri, Ph.D. thesis, Institute for Plasma Research, India, 1991.
[17] S. N. Bhattacharyya and K. Avinash, Phys. Fluids B **4**, 1702 (1992).
[18] M. R. Stoneking, P. W. Fonatana, R. L. Sampson, and D. J. Thuecks, Phys. Plasmas **9**, 766 (2002).
[19] M. R. Stoneking, M. A. Growdon, M. L. Milne, and R. T. Peterson, Phys. Rev. Lett. **92**, 095003 (2004).
[20] H. Saitoh, Z. Yoshida, C. Nakashima *et al.*, Phys. Rev. Lett. **92**, 255005 (2004).
[21] A. W. Trivelpiece and R. W. Gould, J. Appl. Phys. **30**, 1784 (1959).
[22] C. A. Kapetanakos and A. W. Trivelpiece, J. Appl. Phys. **42**, 4841 (1971).
[23] K. Avinash, Phys. Fluids B **3**, 3226 (1991).